Molecular Crystals and Liquid Crystals
Publication details, including instructions for authors and subscription information:
http://www.tandfonline.com/loi/gmcl20

Pentylcyanobiphenyl as Test Molecule for the Acid Sites of Powdered Titanium(IV) Oxides: Sensitivity of Core Levels to the Local Structure

Florica Ungureanu [a], Adrian S. Manea [a], Ligia Frunza [a], Stefan Frunza [a], C. Paul Ganea [a], Florin Cotorobai [a], Lucian Diamandescu [a] & Andreas Schönhals [b]

[a] National Institute of Materials Physics, Magurele, Romania

[b] BAM Federal Institute for Materials Research and Testing, Berlin, Germany

Version of record first published: 30 Jul 2012.

To cite this article: Florica Ungureanu , Adrian S. Manea , Ligia Frunza , Stefan Frunza , C. Paul Ganea , Florin Cotorobai , Lucian Diamandescu & Andreas Schönhals (2012): Pentylcyanobiphenyl as Test Molecule for the Acid Sites of Powdered Titanium(IV) Oxides: Sensitivity of Core Levels to the Local Structure, Molecular Crystals and Liquid Crystals, 562:1, 200-217

To link to this article: http://dx.doi.org/10.1080/15421406.2012.697416

Mol. Cryst. Liq. Cryst., Vol. 562: pp. 200–217, 2012

ISSN: 1542-1406 print/1563-5287 online
DOI: 10.1080/15421406.2012.697416

Pentylcyanobiphenyl as Test Molecule for the Acid Sites of Powdered Titanium(IV) Oxides: Sensitivity of Core Levels to the Local Structure

FLORICA UNGUREANU,[1] ADRIAN S. MANEA,[1] LIGIA FRUNZA,[1,*] STEFAN FRUNZA,[1] C. PAUL GANEA,[1] FLORIN COTOROBAI,[1] LUCIAN DIAMANDESCU,[1] AND ANDREAS SCHÖNHALS[2]

[1]National Institute of Materials Physics, Magurele, Romania
[2]BAM Federal Institute for Materials Research and Testing, Berlin, Germany

Pentylcyanobiphenyl was used successfully as a test molecule to show the acid sites upon some commercial nanoscaled titanium dioxide materials. The surface interactions were investigated in detail using methods sensitive to the surface or to the bulk material, e.g., X-ray photoelectron spectroscopy (XPS), infrared spectroscopy, and thermal analysis. Different oxidation states of surface Ti ions were revealed. Several species were found: the majority were bonded through the nitrogen lone pair of the cyano group, but bonding to the surface OH groups by benzene π electrons might also appear. The N 1s lines of adsorbed 5CB were able to distinguish between Lewis acid and relatively weak Brønsted acid sites.

Keywords Infrared spectra; pentylcyanobiphenyl; size dependence; titanium dioxide; XPS

Introduction

Titanium dioxide (or titania) is widely used for antireflection coatings, gas sensors, as biomaterial, acting as promoter in catalytic reactions, as support for metals and metal oxides, and additive. Especially, it is used as photocatalyst (for a review see, for example, [1]). In addition, the ability of TiO_2 films to align liquid crystal (LC) molecules because of anisotropic dipole–dipole interactions was also investigated [2, 3]. Thus, among the various other potential high dielectric constant oxides, TiO_2 shows an outstanding chemical stability, a high refractive index and UV adsorption.

From the investigation of composite samples containing TiO_2 and 4-pentyl-4′-cyanobiphenyl (5CB) [4] using broadband dielectric spectroscopy, we found that on some titania samples the relaxation rate of the cyanobiphenyl molecules in a surface layer is higher than that of the cyanobiphenyl molecules in the bulk state. Such behavior is not commonly observed for other systems (see e.g., [5]), while other titania composites behave

*Address correspondence to Ligia Frunza, National Institute of Materials Physics, PO box Mg 07, 077125 Magurele, Romania. Tel.: +40 21 3690185; Fax: +4021 3690177. E-mail: lfrunza@infim.ro

Table 1. Bare TiO_2 samples

Sample label	Source	S_{BET} ($m^2\ g^{-1}$)	Phase composition[a]	Calculated 5CB content leading to a monolayer (%)	Physisorbed water[b] (%)
TiK	Kronos	288.0	Anatase (100%)	85.2	2.7
TiG	Degussa P25	53.2	Anatase (85%) Rutile (15%)	51.4	0.7
TiD	Riedel-de Haën	8.2	Anatase (100%)	14.2	< 0.1

[a]Obtained from a detailed analysis of XRD data.
[b]As mass loss up to 400 K by thermogravimetric measurements.

normally as most of the oxide materials, molecular sieves, or aerosil [6, 7], namely the relaxation rate of the molecules in the surface layer is lower than that in the bulk 5CB.

On the other hand, pentylcyanobiphenyl molecules that are adsorbed on the surface of TiO_2 (anatase) nanoparticles result in species hydrogen bonded through the nitrogen lone pair of the cyano group and species bonded by π electrons of the benzene rings [8], as observed by infrared spectroscopy.

Assuming a selective behavior of the multifunctional organic molecules at the TiO_2 surface, this article considers in detail the surface species of 5CB/TiO_2 composites by a combination of methods, such as thermal analysis, infrared spectroscopy, and X-ray photoelectron spectroscopy (XPS), sensitive either to the bulk material or to a surface layer with a thickness of a few nm. This behavior was expected to discriminate between the species bonded by aromatic π electrons, the nitrogen electron lone pair, π electrons of the CN group, or the benzoimine-like species as it was found for adsorbed benzonitrile [9]. A core-level XPS study is reported, which focuses on the detailed analysis of the O 1s, N 1s, C 1s, and Ti 2p peaks. The quantitative evaluation reveals different oxidation states of the surface Ti ions on the TiO_2 samples; the samples with higher Ti binding energies lead to chemical modifications of the 5CB molecules.

Experimental Techniques

The samples were TiO_2-based catalyst powders provided by Kronos, Degussa, and Riedel-de Haën. Their labels and some properties are collected in Table 1.

Nitrogen adsorption was employed to estimate the Brunauer Emmett-Teller (BET)-specific surface area (S_{BET}) of these oxides. The S_{BET} value in TiD sample (Table 1) is smaller and in TiG sample it is 53.2 $m^2\ g^{-1}$ as per the literature data [10–12]. The TiK sample has the highest surface area (see Table 1).

The 5CB (Fig. 1) is a thermally stable single-component LC. In the bulk, 5CB shows the well-known phase transitions at

$$Cr \rightarrow 297\ K \rightarrow N \rightarrow 308.5\ K \rightarrow I,$$

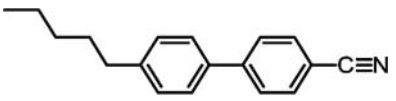

Figure 1. Chemical structure of 5CB.

where *Cr* symbolizes the crystalline state, *N* is the nematic, and *I* is the isotropic state. The 5CB was purchased from Aldrich and was used without further purification.

Dispersal of the 5CB molecules on the catalyst surface was performed by mixing the TiO_2 powder with the appropriate amount of 5CB solved in carbon tetrachloride. Details of the method are given elsewhere [6]. The solvent was then removed in vacuum at 348 K, for 24 h. Its complete removal was checked by blank experiments. This method allows to reach high values of the TiO_2/5CB ratio leading to 5CB monolayer.

To obtain samples with different loading levels, different concentrations of the 5CB solution were prepared. The content of 5CB in the composites was determined by thermogravimetric (TG) measurements as already described for other composites [13]. The amount of the organic material is measured by the weight loss up to 723 K, while the inorganic oxide remains stable up to much higher temperatures (the weight should be almost constant by increasing the temperature up to 973 K or higher). From that weight loss the layer thickness was estimated. The TG measurements were performed with a Perkin–Elmer Diamond TG-DTA equipment, under dry air atmosphere with a heating rate of 10 K min^{-1}. In the following, the composite samples were labeled by 5CB(*n*)/Ti*M*, where *n* is the 5CB/TiO_2 ratio and *M* labels the source of the TiO_2 material (see Table 1). Table 2 shows the codes and the TG data of the composites.

The structure of titanium dioxide materials was investigated by X-ray diffraction using a Bruker D8 Advance Diffractometer (CuK_α radiation with $\lambda = 1.5406$ Å).

X-ray photoelectron spectroscopy was used to characterize the surface of the nanostructured TiO_2 materials and their composites. The studies were carried out with an updated spectrophotometer VG ESCA MKII, with an Al source ($K_\alpha = 1486.6$ eV), at a take-off angle of 55° [14], using SDP 32 and S-PROBE software. Peak positions were assigned by referencing the C 1s peak (adventitious carbon) to a binding energy of 285 eV and a linear shift of all other peaks by an equal value, as customary. Both survey and narrow window scans of Ti 2p, C 1s, N 1s, and O 1s peaks were conducted at 50 eV pass energy, with an energy increment of 1 eV for survey and 0.05 eV for the narrow window scans [15,16]. Shirley backgrounds were used in all fits to the narrow scan spectra. Fits were carried out where line shape, peak width and binding energy were adjustable parameters. Because of the conducting properties of TiO_2, electrons were not supplied for charge compensation. No in situ cleaning was applied to the samples before measuring.

Vibrational spectra were recorded at room temperature with a FTIR Spectrum BX (Perkin–Elmer) spectrometer in KBr, or using self-supported pellets. A standard measuring

Table 2. Properties of the composites

Sample label	5CB/TiO_2 weight ratio[a]	5CB content[b] (%)	Physisorbed water[b] (%)
5CB(0.200)/TiD	0.200	17.4	–
5CB(0.067)/TiD	0.067	5.7	–
5CB(0.227)/TiG	0.227	18.5	0.4
5CB(0.120)/TiG	0.120	10.4	0.5
5CB(0.200)/TiK	0.200	31.8	2.6
5CB(0.067)/TiK	0.067	13.6	3.7

[a]At the preparing stage.
[b]By thermogravimetric analysis.

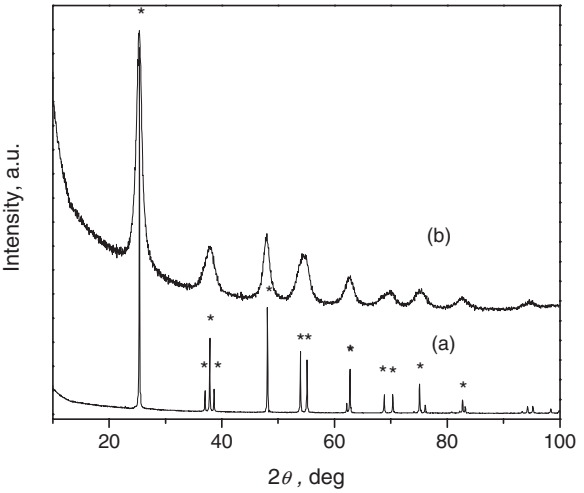

Figure 2. X-ray patterns of (a) TiD; (b) TiK samples. The asterisks give the positions of the anatase peaks among the main observed peaks.

of a sample/KBr pellet (the same amount of sample and KBr, the same pressure value, etc.) was adopted for a first comparison of the spectra. The obtained spectra were analyzed in detail by fitting Gaussians to the data. Attenuated total reflection (ATR) measurements were also performed.

Results and Discussion

The results are discussed in the following sequence: the crystalline structure of the powdered oxides is considered. Then, the data obtained by thermal analysis, XPS, and FTIR spectroscopy were described for both bare oxides and for composites. When possible, these results were correlated to give a unified view on the surface interactions.

XRD Investigation of the Bare TiO_2 Powders

Figure 2 presents a comparison of the XRD patterns obtained for TiD and TiK samples. The most intensive diffraction peaks in these XRD patterns are assigned to the anatase crystal structure (SG 141, I41/amdZ). The absence of peaks at $2\theta = 27.5^\circ$ and 30.8° due to (110) and (121) reflections of rutile (SG 136, P42/mnm) and brookite [17], respectively, indicates that these phases are not present. The intense lines of the TiD sample reveal a high degree of crystallinity, while the broad diffraction peaks of TiK sample indicate the nanometric dimensions of the particles.

Detailed structure determination was performed by the Rietveld method [18] in order to obtain quantitative results related to the properties of TiO_2 nanopowder. The crystallite size was calculated using the Scherer's equation, and the sequence of the estimated values is in good agreement with S_{BET} specific areas (see Table 1). The obtained average crystallite size and lattice parameters are summarized in Table 3. Two phases (anatase and rutile) were found to exist simultaneously for the TiG sample (Degussa P-25), which was also reported in [19,20]. But the main part of the material (85%) has an anatase phase as in the case of two other samples. The weighted average particle size was calculated to 38.1 nm.

Table 3. Results of Rietveld refinement of the oxide structure

	Lattice parameters		
Sample	*a* (Å)	*c* (Å)	Particle size (nm)
TiD	3.7828	9.5068	140
TiG	3.7892[a]	9.5172[a]	33
	4.5978[b]	2.9600[b]	67
	Weighted average		38.1
TiK	3.7986	9.5165	9.4
Errors	±0.0005	±0.0005	±0.2

[a]Anatase.
[b]Rutile.

TG Investigations

TG analysis of bare TiO_2 samples was employed to detect the total weight loss due to physically and chemically bound water. TG curves are shown in Fig. 3: heating up to 400 K removes the physically adsorbed water (e.g., [21] and references cited therein). This first step is not crucial for characterization of the powders as it depends on humidity during sample keeping and handling. As expected, the amount of the desorbed water (estimated by the weight loss up to 400 K) scales with the specific surface area (see Table 1). The second step of the weight loss (heating up to ∼800 K) generally represents the removal of OH groups from the surface, and possibly desorption of volatile organic compounds associated with powder processing. The last step is used to determine the carbon content of the oxide powder. At higher temperature, a phase transformation from anatase to rutile [17] takes place and the heat flow curve (not shown here) shows an exothermal peak. Additionally, the oxidation of some Ti^{3+} ions to Ti^{4+} might as well slightly increase the mass.

The density of the OH groups at surface (leading to the desorption of bound water at temperatures higher than 500 K) for a fully hydroxylated titania powder consisting of

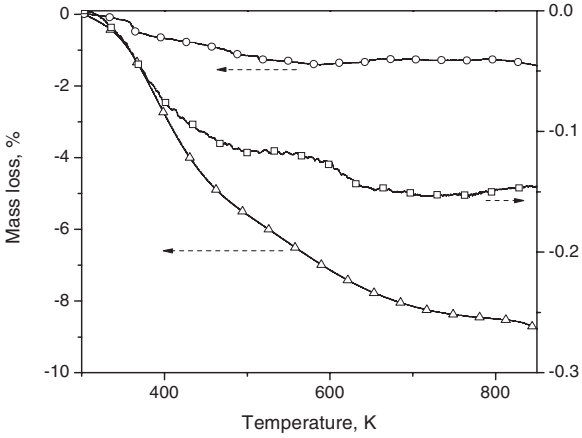

Figure 3. TG plots of the bare samples: □ – TiD (right *y*-scale), ○ – TiG (left *y*-scale), and △ – TiK (left *y*-scale).

anatase with a (111) lattice structure was found to be 12–14 OH/nm^2 [22], while for a Degussa P25 sample it is 3.3 OH/nm^2 (by XPS analysis) [11]. Such a picture of the surface composition should be realistic in the case of our sample TiG because these samples are based on P25 material.

Thus, we found that the main decomposition peak of bulk 5CB is at 615 K; two other processes of small intensity appear before (460 K) and after this temperature (845 K) as expected [23]. Representative TG plots of samples loaded with 5CB are given in Fig. 4. There are several steps in the mass loss, which can be seen in the derivative thermogravimetry (DTG) curves. These DTG peaks are asymmetric, which reveals that several species that are differently bonded to surface contribute to the mass loss. Additionally, the processes have a higher or lower rate depending on the surface interactions, which in turn are due to the nature of the catalyst and the thickness of the CB layer. Thus, for the same TiO_2/5CB ratio, different samples have a similar decomposition pattern but with different relative intensities for different processes. One process is found at lower temperatures (process 1) than the main decomposition for bulk 5CB (below 600 K), while the second process (process 2) is found at higher temperatures above 700 K. The temperature positions and the relative intensities of these two processes depend on the specific surface areas or the sizes of the particles (see Table 3). Decreasing the layer thickness (higher TiO_2/5CB ratio) leads to a decrease in the relative intensity of the low temperature peak and an increase of the second peak.

To discuss the decomposition behavior of different samples the DTG curves are plotted together for the same TiO_2/5CB ratio in Fig. 5. With increasing specific surface area of the particles (decreasing particle size), process 1 shift to lower temperatures and decreases in its relative intensity. Process 2 increases in its relative intensity with increasing surface area and also slightly shifts to lower temperatures. Moreover, because the samples with the same 5CB content are compared and the amount of 5CB used for the formation of a monolayer increases with increasing surface area, process 2 is used for the decomposition of a layer of 5CB molecules close (in strong interaction) to the surface of TiO_2, while process 1 is more of bulk-like because of the distance of molecules from the surface. Process 1 is shifted to lower temperatures in comparison to bulk 5CB because of the absence of layer interactions in liquid and stabilized molecule. Therefore, process 1 shifts to lower temperatures when there is a decrease in the number of bulk-like molecules.

Furthermore, when the behavior of these 5CB/TiO_2 samples is compared with that of the 8CB/SiO_2 composite systems containing a homolog of 5CB deposited onto aerosil [13], one observes that although the temperature of the main decomposition process takes place at 636 K for the bulk cyanobiphenyl, it appears at up to 70 K for the composites with the monolayer coverage. DTG curves are also asymmetrical and depend on the cyanobiphenyl amount. Hydrogen bonding of the cyanobiphenyl molecules with the surface was verified in all these 8CB/SiO_2 cases. However, a variety of interactions of 5CB with TiO_2 surface are expected from spectroscopic investigations [8] of related composites. These bondings lead to differently shaped DTG curves and hamper a quantitative comparison.

A more unambiguous assignment of the above-mentioned thermal processes can be done only by coupling the TG measurements with investigations that identify the desorption products. Such investigations are proposed but not yet in progress.

The loading degree calculated on the basis of the thermograms (see Table 2) is low and ensures a thin layer approaching the thickness of a monolayer. The amount of 5CB necessary to form a monolayer can be estimated by considering the specific surface area of the TiO_2 material, assuming the orientation of the 5CB molecules perpendicular to the surface and using the length of unfolded 5CB molecule as the layer thickness [13]. The as-calculated values are given in Table 1. Thus, due to the large surface-to-volume ratio of

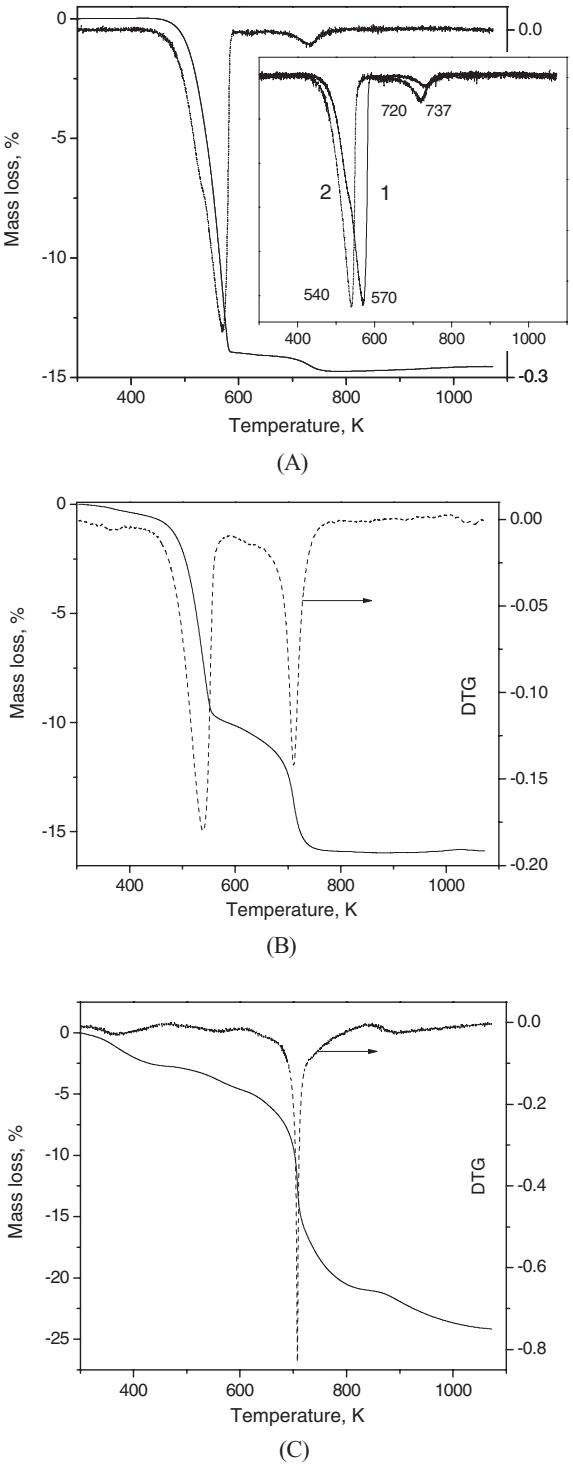

Figure 4. TG–DTG plots for the samples as follows: (A) 5CB (0.200)/TiD; (B) 5CB (0.227)/TiG; and (C) 5CB (0.200)/TiK. The insert shows the main processes in the DTG curves for composites with different TiD/5CB ratios: (1) 5; (2) 15.

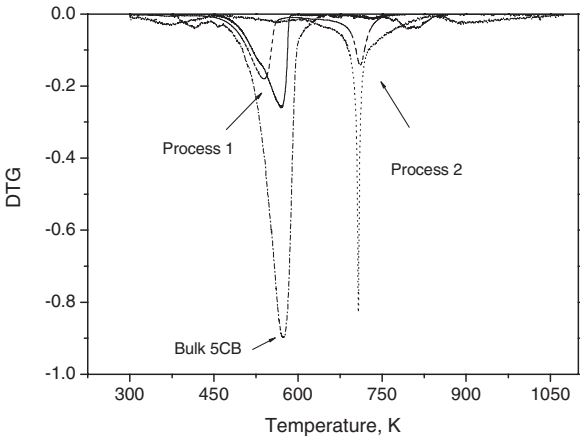

Figure 5. Comparison of the DTG curves for representative samples: solid line – 5CB (0.200)/TiD; dashed line – 5CB (0.227)/TiG; and dotted line – 5CB (0.200)/TiK. The behavior of bulk 5CB (dash-dot line) is also added where the absolute values where scaled by a factor 0f 0.5 for sake of clearness.

the composites, the 5CB molecules in the surface layer have the largest contribution to the observed behavior.

X-ray Photoelectron Spectroscopy

Bare Oxide Samples. X-ray photoelectron survey spectra (not shown here) of the bare oxide samples reveal the surface composition of the investigated samples. The elements present at the surface were only C, O, and Ti, indicating that the contaminations are due to organic adsorbates.

High-resolution photoelectron spectra in the energy region, where titanium and oxygen peaks appear, are given in Fig. 6 along with the peak decomposition in the corresponding insets. For the fit functions, either Gaussians (in the case of Ti) or combined 60% Gaussian –40% Lorentzian (in the case of O) are employed.

The position of Ti peaks is shifted to higher values of the binding energy according to the sequence TiD < TiG < TiK. This means that the binding energy of Ti is higher for smaller particles than for larger ones. This systematic shift of the binding energy correlates well with the shift found for O1s core level (see further). Although one cannot exclude surface charge, which might be slightly different for the investigated samples, this shift can be more likely due to the adsorption of organic molecules on the particle surface, which shifts the position of the peak.

The spin–orbit components ($2p_{3/2}$ and $2p_{1/2}$) of each peak could be well described by only one curve, corresponding to titanium dioxide [24–27]. The peak separation of 5.5–5.9 eV between the Ti $2p_{1/2}$ and Ti $2p_{3/2}$ signals is in agreement with literature values [28]. The components of the Ti $2p_{3/2}$ peak (three components were sufficient to describe the data for each sample) might be attributed mainly to Ti–OH (458 eV), and especially to bulk TiO_2 (459.3 eV) [29–32]. Some species (at 457 eV) might be due to Ti_2O_3. Ti^{3+} is expected because TiO_2 usually have oxygen vacancies and therefore Ti^{3+} ions in the lattice. However, Ti^{3+} appears in a very low concentration for our samples. The peaks of Ti atoms (454 eV) and of TiO (455.2 eV) seem to be absent for our materials. The peak position shifts

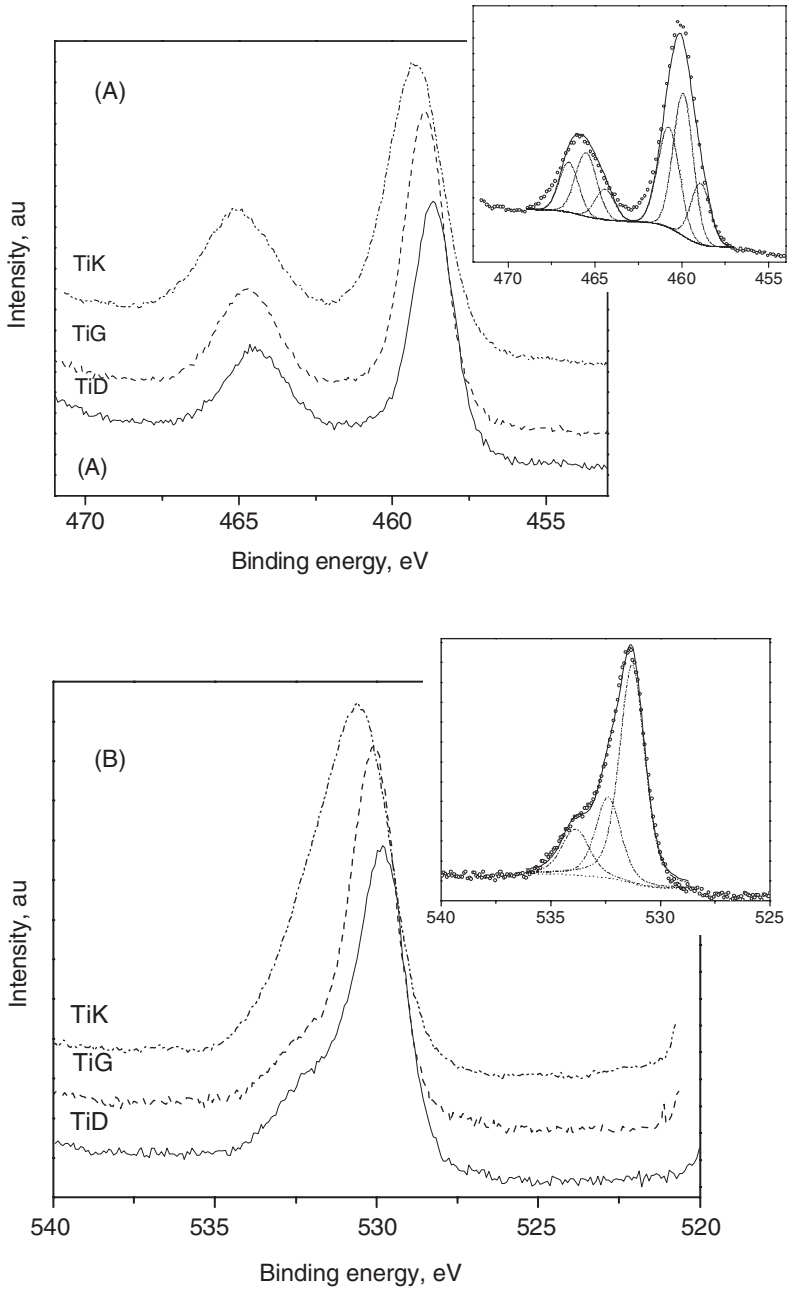

Figure 6. Titanium (A) and oxygen (B) XP spectra of the investigated samples. Each spectrum has been scaled separately for sake of clearness. The inserts show the decomposition of the peaks for the TiD sample, Shirley background is included as solid curve at peak base.

as function of the presence of adventitious carbon (or 5CB, see below) because organic molecules adsorb at the surface of the particles. For smaller particles, a higher amount of molecules can adsorb. This is verified by an increased total intensity of the C 1s peak (see

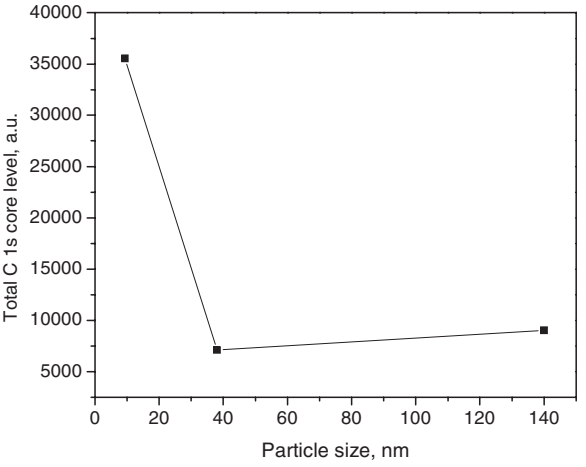

Figure 7. Total intensity of C 1s core level of the oxide samples as function of their particle size.

Fig. 7) and a larger shift in the peak position is observed. The full width at half maximum (fwhm) is comparable for the same species using the value given in the literature for Ti compounds. The percentage of the species is illustrated in Fig. 8 as function of the particle size.

The locations of the binding energies for the peaks, which create the O 1s signal, agree well with the reported values for bulk oxide (O^{2-}) and hydroxyl (OH^{-}) species [11,28,33–35]. The values of the fwhm of the higher and lower binding energy peaks were 1.30 and 1.68 eV, respectively. The difference between the binding energies of the assigned hydroxyl (OH^{-}) and oxide (O^{2-}) species was approximately 1.2 eV, which is close to the reported differences of (1.24) 1.5–1.9 eV. A direct comparison with the data for soda glasses recently discussed by Nesbitt et al. [36] cannot be done, but one can adapt their conclusion that three (or more) different oxygen types can exist as well. Thus, the major contribution located at 531 eV, a value usually reported for TiO_2 samples arises from the bulk O^{2-} oxygen atoms ([37] and the literature cited therein). Also according to the cited literature the peaks at 532.2 eV and 533.3 eV can be well addressed to the twofold and single-fold oxygen atoms, respectively.

The difference in the binding energy (of 71.2 eV) between the peak positions of Ti $2p_{1/2}$ and O 1s (oxide) is also in excellent agreement with reported literature values between 72.9 eV and 71.2 eV [34, 35, 38, 39].

Composite Samples. Representative narrow scan XP spectra of the composite samples are shown in Fig. 9 for the binding energy regions of titanium and oxygen.

Curve analysis of the O 1s signal for the composites indicated the same number of peaks as for the unloaded oxides: Therefore, the peaks were assigned in a similar manner. Because O 1s photoelectrons from oxide and hydroxyl ions have nearly the same kinetic energy, the 5CB surface layer does not significantly affect the ratio of the signal intensities I_{OH}/I_{oxide}. As a first result, the spectra appear to contain significant amount of hydroxyl groups at the surface, although 5CB was adsorbed. Therefore, a quantitative comparison of the percentage of hydroxyl groups at the surface of TiO_2 and the composite particles is more suitable than a comparison of their intensities. This ratio increases for composites,

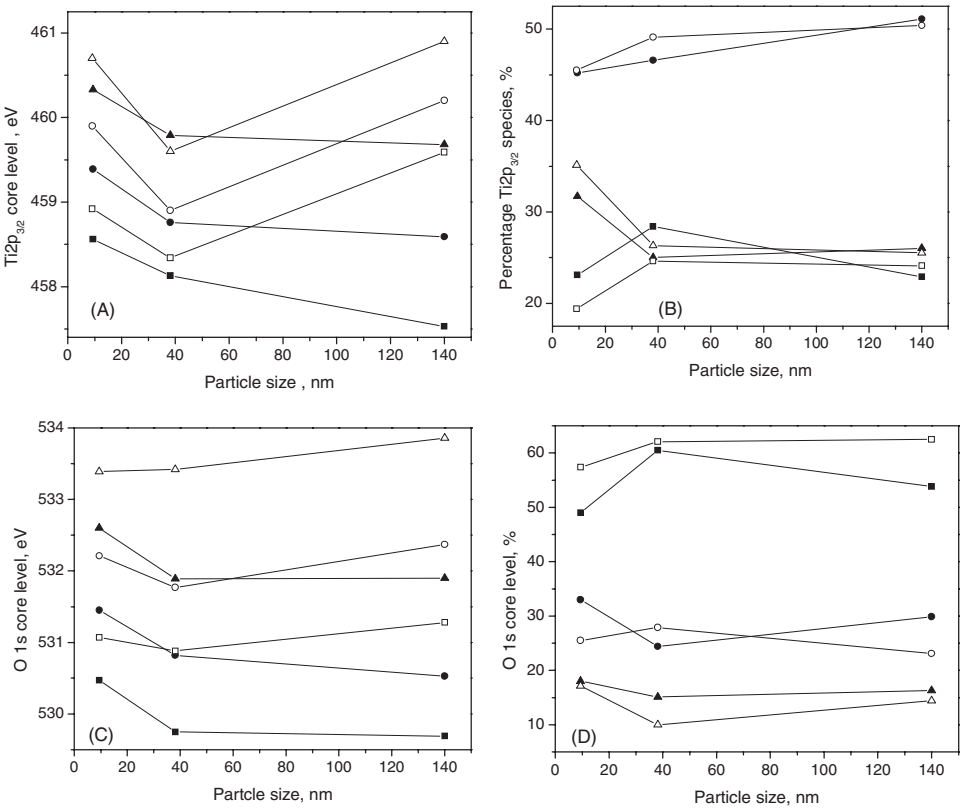

Figure 8. Intensity and position of Ti $2p_{3/2}$ and O 1s core levels of the composite samples with the ratio 5CB/TiO_2 = 0.067 (filled symbols) in comparison with the core levels of the corresponding oxide samples (empty symbols) as function of their particle size.

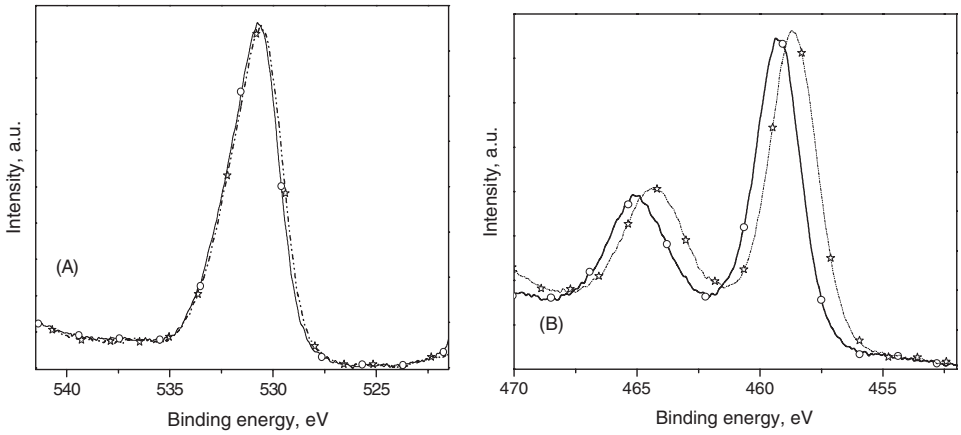

Figure 9. XP spectra of (A) O 1s core level and (B) Ti $2p_{3/2}$ core level for the 5CB(15)/TiK sample (continuous line) in comparison with those of the corresponding oxide sample (dash-dotted line). The ordinate scale is shifted for one sample against the other in both cases A and B for sake of clearness.

by decreasing the percentage of the oxide ions and also by increasing the percentage of the OH ions—at the same time, the amount of the third oxygen species is also changed (Fig. 8).

The (organic) molecule–surface interactions may strongly influence the core-level binding energies of the O 1s core level in the titania layer. Thus, binding energy of 531.6–532.1 eV is typical of hydroxyl groups at bridging sites [40–42].

The O and Ti photoemission spectra from the composite samples are shown in Fig. 9. However, the intensity of the O and Ti photoelectrons is slightly reduced when compared with the oxides as expected due to the presence of the surface 5CB layer. We found that the position of the O 1s is shifted approximately 0.2 eV as compared with those in pure oxides. In addition, the Ti peak positions are shifted approximately 1 eV toward lower binding energies. This shift can be understood by considering that the surface of the particles has certain roughness with exposed parts. As a consequence, some 5CB molecules are bonded to these exposed centers. For this, one may conclude that the 5CB molecules bonded by the Ti ions can be better identified than those bonded by hydrogen bonding onto terminal oxygen atoms.

Further, it was observed (not shown here) that the intensity of the C 1s signal increases slightly but systematically for the composites when compared with the corresponding oxide sample. This increase is due to the 5CB surface layer, but unfortunately the layer thickness cannot be estimated on this basis. Moreover, despite the fact that the C 1s peak was resolved by curve fitting into three components, their assignment to the carbon atoms in the CN group, to the carbon bonded to the cyano group, and to the other carbon atoms knowing the C 1s binding energies of gaseous benzonitrile (at 292.2, 291.9, and 291.0 eV respectively [43]) is not straightforward. The assignment of C 1s peak components to the benzoimine species probably formed onto the oxide surface is also not obvious (see ref.[9] and the discussion below).

Instead, the 5CB coordination can be more easily seen in the N spectrum. Fig. 10 shows representative spectra for two TiD containing samples with different concentration of 5CB.

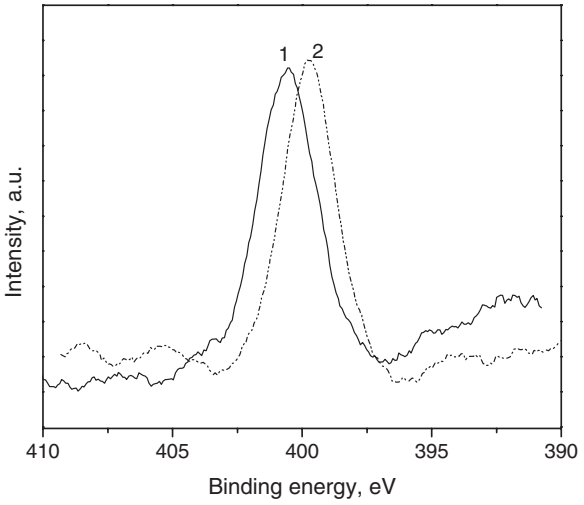

Figure 10. N 1s XP spectrum for samples with different concentrations of 5CB: 5CB (0.020)/TiD (solid line) and 5CB(0.067)/TiD (dotted line).

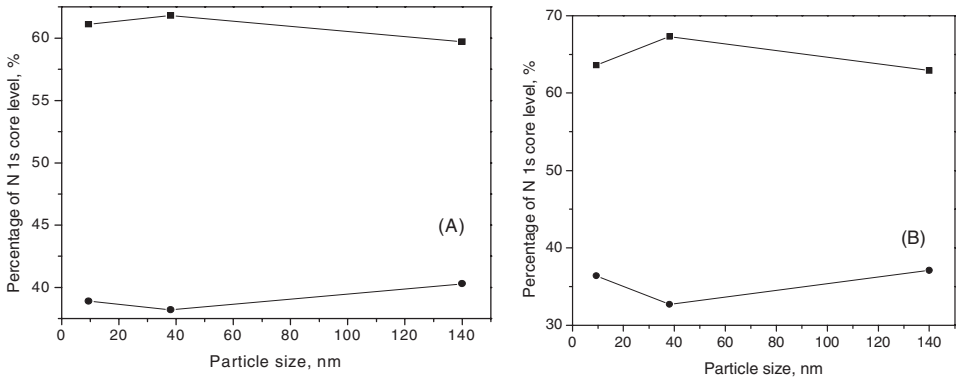

Figure 11. Percentage of N 1s core level of the composite samples with the ratio 5CB/$TiO_2 = 0.067$ (A) in comparison with the core levels of the samples with the ratio 5CB/$TiO_2 = 0.200$ (B) as function of their particle size.

At least two 5CB surface species could be found on TiO_2 surface taking into consideration the values of the N 1s core-level binding energies of pyridine adsorbed onto molecular sieves [44, 45], both bonded by the nitrogen electron lone pair: one species bonded to the surface cations with an empty orbital (so called Lewis acids) leading to binding energy at approximately 399 eV and a second one, at higher binding energy, bonded to the Bronsted acid sites (proton donor surface OH groups). Indeed, two 5CB species were found by deconvolution of the N 1s core level on the surface of the investigated TiO_2 samples: these species put in evidence Lewis sites and weak Bronsted sites. Moreover, our composite samples containing a very low amount of 5CB on TiK oxide material, approach values that might be associated to less weak Bronsted acids. The dependence of the two 5CB species on the particle size appears in Fig. 11: for both loadings the distribution of the N species is almost similar.

FTIR Investigations

A representative infrared spectrum of a TiO_2 oxide (TiD) and a corresponding composite sample is presented in Fig. 12.

There are strong and overlapping absorptions between 400 cm^{-1} and 1000 cm^{-1} [not shown in Fig. 12(A)] in the spectrum of TiO_2 oxides. In this region, the stretching vibrations of the Ti–O bonds (550–653 cm^{-1}) and of the Ti–O–Ti bonds (436–495 cm^{-1}) [46] appear. In addition, in the same wave number range there are the vibrations of the surface groups (700–1300 cm^{-1}), hydroxyl and metal–oxygen bonds, and different dopants. Between 1000 cm^{-1} and 1300 cm^{-1}, a broad absorption [Fig. 12(A)] includes the peaks appearing at 1048 cm^{-1}, 1137 cm^{-1}, and 1222 cm^{-1} related to the δ(Ti–O–H) deformation vibrations, also called longitudinal and transverse optical phonons [47]. However, the assignment of the peaks due to the vibrations of the groups of the TiO_2 framework is beyond the scope of this work, therefore we focus only on the bands, which are involved in the interactions of 5CB molecules with the surface groups of TiO_2.

Figure 12(A) shows a narrow peak at 3695 cm^{-1} (which is due to the stretching mode νOH of free hydroxyl groups) followed by a broad adsorption region at lower wave numbers down to approximately 3000 cm^{-1}; the latter band can be decomposed into several components owing to νOH of hydrogen bonded hydroxyl groups and to the symmetric and

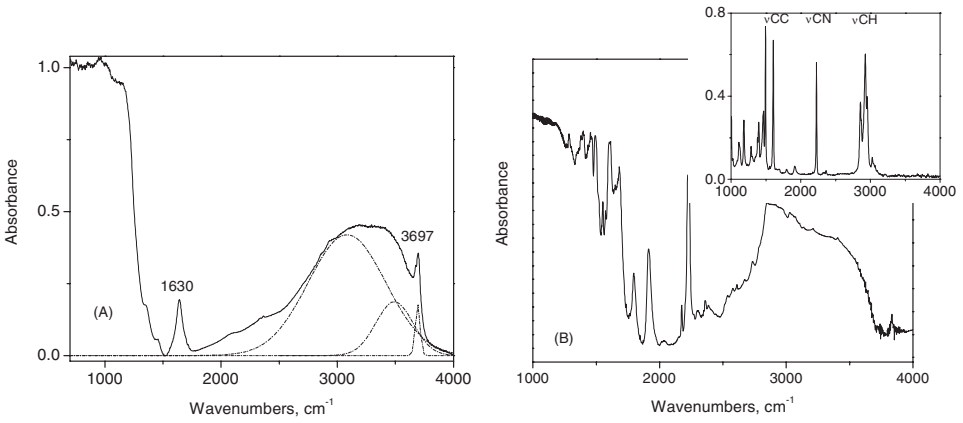

Figure 12. FTIR spectrum of the TiD sample (A) and of a corresponding composite 5CB (0.200)/TiD (B). The insert gives the spectrum for bulk 5CB together with the assignments of its main peaks.

antisymmetric νOH modes of molecular water coordinated by different types of Ti^{4+} ions [48–55]. Free OH (unbounded) groups do not appear any longer in the spectra of the composites [Fig. 12(B)].

The IR spectra of the composites are containing peaks due to both TiO_2 and 5CB. Similar to TiO_2, the composite [Fig. 12(B)] also shows a strong and broad OH stretching peak between 3000 cm^{-1} and 3800 cm^{-1} but with a different spectral shape than for the case of bare oxide. This change in the spectra is due to the OH stretching vibration: hydroxyl groups of the titania material can be bonded in the composite either to the nitrogen lone pair of the cyano groups or to the π electrons of the aromatic rings in the cyanobiphenyl molecules. These bondings shift the stretching OH frequency to lower wave numbers and explain the disappearance of the peak characteristic to free OH groups.

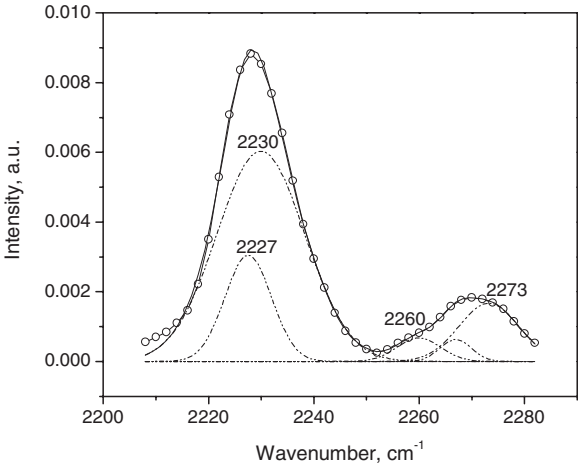

Figure 13. Analysis of the absorption in the CN stretching region for the sample 5CB (0.200)/TiK. Points are experimental data; the dotted lines show the Gaussian components; and the solid line is the sum of these components.

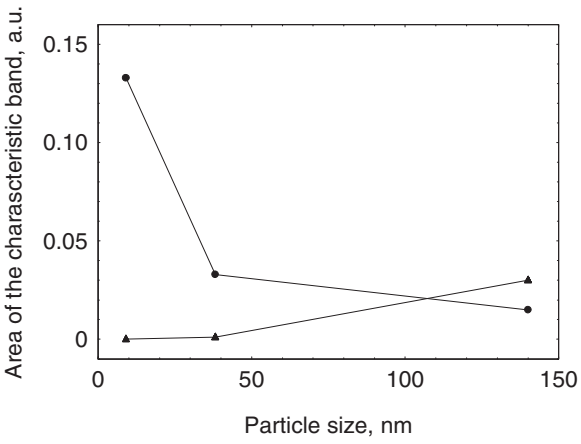

Figure 14. Area of the characteristic cyano bands in the composite samples with thicker 5CB layer, as function of the particle size: • – 5CB species coordinated to Ti ions; ▲ – 5CB species hydrogen bonded to OH groups.

In the wave number, region between 2000 cm^{-1} and 2500 cm^{-1} of the oxide framework does not have strong IR absorptions. Therefore, some peaks can be clearly identified [Fig. 12(B)] as belonging to 5CB, and according to the rich literature on bulk cyanobiphenyls, they are related to nitrile compounds and also to their interaction with different surface adsorption sites [7, 23, 56–62]. This identification first concerns the C=N stretch (at ca. 2226 cm^{-1}). Other peaks that can be well observed and assigned are the peaks due to asymmetrical and symmetrical stretch of CH bonds in CH_3 and CH_2 groups (between 2956 cm^{-1} and 2857 cm^{-1}), those due to CC aromatic ring stretch (at 1606 cm^{-1} and 1494 cm^{-1}), to alkyl deformation (at 1460 cm^{-1}, 1397 cm^{-1}, and 1378 cm^{-1}), and those due to the stretch of C–C biphenyl bridge (at 1285 cm^{-1} cm^{-1}). It is worth noting that the C=N stretching mode at 1629 cm^{-1} cannot be easily distinguished in the spectra of our samples due to its overlapping with the TiO_2 matrix band and with water deformation appearing at the same position.

The complex peak due to stretching vibration of the CN group is analyzed by fitting Gaussians to the data where the number of applied Gaussians depends on the sample. Representative example of the fitting process is given in Fig. 13.

This band shape analysis has shown that there are several peaks assigned to 5CB molecules as follows: a peak at ca. 2226 cm^{-1} broader than the band of the monomers [56] is due to bulk-like dimers. It is known that dimers of 5CB molecules in the bulk are well proved [63], mostly by XRD studies. A narrow peak at 2227 cm^{-1} is assigned to bulk-like monomers while the one at ca. 2235 cm^{-1} is related to hydrogen bonded molecules Ti–OH ... NC–. Here, the bonding takes place through the lone nitrogen pair of the cyano group. The peak at ca. 2265 cm^{-1} is due to coordinately bonded molecules Ti ... NC–: For example, for benzonitrile complex with Ti ions the upward shift is of ca. 40 cm^{-1} [64]. Coordination through the π system of the CN group [8] generally results in a decrease of the CN stretching frequency to $\sim$2222 cm^{-1}; however, this type of bonding is less evident in our samples. The benzene rings of adsorbed 5CB molecule might be oriented parallel to the oxide surface [65], but this behavior is still undetermined from our experiments. More systematic investigations would be necessary to unravel all the surface species developed by the molecules of 5CB onto the catalytically active powdered TiO_2 samples.

Figure 14 shows the dependence of the amount of 5CB species as function of the particle size of the pure oxides: it seems that the large particles have less exposed Ti ions to bond the cyano groups of 5CB molecules, whereas they have more OH groups that are able to form hydrogen bonds in these 5CB molecules. These data show another finding for the thermodynamic correlation of the size effect with the adsorption of molecules in nanocrystals [66].

Conclusions

Pentylcyanobiphenyl has been chosen to interact with the surface of some powdered commercial TiO_2 catalysts because of its multifunctional molecules with high thermal stability. Before the interaction with this test molecule is considered, titania materials were well characterized by XRD coupled with Rietveld analysis, nitrogen absorption, thermal analysis, and XPS. Different oxidation states of the surface Ti ions were revealed, as expected.

The features of the surface species of 5CB were determined from the investigations by infrared spectroscopy, XPS, and thermal analysis.

Thermal analysis applied to composites containing TiO_2 and 5CB did not reveal interactions at the microscopic level, but allowed inferring some information concerning the structure of the surface layer. The profiles of TG curves obtained in the case of composite samples presumably reflect desorption and decomposition from different types of surface microdomains, that is, with different 5CB–substrate interactions. However, it is now difficult to identify such domains.

The complex shape of the TG curves for the composite samples shows differences in the temperature at the maximal loss for each temperature interval, and dependence on the TiO_2/5CB ratio.

Core level XPS lines were well resolved into components. The analysis of N 1s core level put in evidence different acid sites on the surface of our TiO_2 samples: coordinatively unsaturated titanium Lewis sites and weak proton donor OH groups as Bronsted sites.

Band shape analysis was performed for characteristic IR peaks (especially to those due to CN or OH stretching vibrations). Several species resulted from 5CB by interaction with the surface and were clearly put in evidence in the region of CN stretching, such as hydrogen bonded molecules and coordinately bonded molecules through the nitrogen lone pair, species that correlate well were found from XPS analysis.

Bonding of 5CB molecule through π-electron clouds of benzene rings is quite possible but was not clearly demonstrated in our experiments.

Due to the particular interaction with the TiO_2 surface, pentylcyanobiphenyl can be taken as a test molecule, because it has good affinity for the surface of oxide nanocrystals and spectroscopic properties to distinguish the nature and the distribution of the acid sites.

Acknowledgments

The authors thank the Romanian Ministry of Education and Research for financial support by the Project COMAFI of the CORE Program. Valuable discussions with M. F. Lazarescu (NIMP) and the BET measurements performed by B. Cojocaru (Bucharest University) are highly appreciated.

References

[1] Carp, O., Huisman, C. L., & Reller, A. (2004). *Progr. Solid State Chem.*, *32*, 33.

[2] Okutan, M., Yakuphanoglu, F., Kösal, O., San, S. E., & Oweimreen, G. A. (2008). *J. Non-Cryst. Solids*, *354*, 3529.

[3] Lee, J.-W., Moon, B.-M., Lee, K.-M., Kim, Y.-H., Park, H.-G., Lim, J.-H., Oh, B.-Y., Kim, B.-Y., Hwang, J.-Y., Ok, C.-H., Seo, D.-S., & Han, J.-M. (2010). *Liq. Cryst.*, *37*, 279.
[4] Frunza, L., Frunza, S., & Schönhals, A. (in preparation); Ungureanu F., Frunza, L., Frunza, S., Ganea, P., Cotorobai, F., Logofatu, C., Lazarescu M. (2010). Oral Presentation at the 9th Symposium of the Romanian Catalysis Society, June 23–26, Iassy, Romania.
[5] Leys, J., Glorieux, C., & Thoen, J. (2008). *Phys. Rev. E*, *77*, 061707; Leys, J., Glorieux, C., & Thoen, J. (2010). *J. Non-Cryst. Solids*, *356*, 597.
[6] Frunza, S., Schönhals, A., Frunza, L., Zubowa, H.-L., Kosslick, H., Fricke, R., & Carius, H. (1999). *Chem. Phys. Lett.*, *307*, 167; Frunza, L., Frunza, S., & Schönhals, A. (2000). *J. Phys. IV France*, *10*, Pr7-115.
[7] Frunza, S., Frunza, L., Tintaru, M., Enache, I., Beica, T., & Schönhals, A. (2004). *Liq. Cryst.*, *31*, 913.
[8] Bezrodna, T., Puchkovska, G., Shimanovska, V., & Baran, J. (2004). *Mol. Cryst. Liq. Cryst.*, *413*, 71.
[9] Nakayama, T., Inamura, K., Inoue, Y., Ikeda, S., & Kishi, K. (1987). *Surf. Sci.*, *179*, 47.
[10] Tanaka, K., Capule, M. F. V., & Hisanaga, T. (1991). *Chem. Phys. Lett.*, *187*, 73.
[11] Erdem, B., Hunsicker, R. A., Simmons, G. W., Sudol, E. D., Dimonie, V. L., & El-Aasser, M. S. (2001). *Langmuir*, *17*, 2664.
[12] Yamakata, A., Ishibashi, T., & Onishi, H. (2007). *Chem. Phys.*, *339*, 133.
[13] Frunza, S., Kosslick, H., Schönhals, A., Frunza, L., Enache, I., & Beica, T. (2003). *J. Non-Cryst. Solids*, *325* 103.
[14] Negrila, C. C., Logofatu, C., Ghita, R. V., Cotirlan, C., Ungureanu, F., Manea, A. S., & Lazarescu, M. F. (2008). *J. Crystal Growth*, *310*, 1576.
[15] Ghita, R. V., Negrila, C. C., Ungureanu, F., & Logofatu, C. (2010). *Optoelectron. Adv. Mater.-Rapid Commun.*, *4*, 1736.
[16] Samide, A., Ciuciu, A., Logofatu, C., & Preda, M. (2010). *Mater. Plast.*, *47*, 173.
[17] Bhattacharyya, A., Kawi, S., & Ray, M. B. (2004). *Catal. Today*, *98*, 431.
[18] Diamandescu, L., Vasiliu, F., Tarabasanu-Mihaila, D., Feder, M., Vlaicu, A. M., Teodorescu, C. M., Macovei, D., Enculescu, I., Parvulescu, V., & Vasile, E. (2008). *Mater. Chem. Phys.*, *112*, 146; Vasiliu, F., Diamandescu, L., Macovei, D., Teodorescu, C. M., Tarabasanu-Mihaila, D., Vlaicu, A. M., & Parvulescu, V. (2009). *Topics Catal.*, *52*, 544.
[19] Hurum, D. C., Agrios, G. A., Gray, A. K., Rajh, T., & Thurnauer, C. M. (2003). *J. Phys. Chem.*, *107*, 4545.
[20] Maiyalagan, T., Vishwanathan, B., & Varadaraju, U. V. (2006). *Bull. Mater. Sci.*, *29*, 705.
[21] Mueller, R., Kammler, H. K., Wegner, K., & Pratsinis, S. E. (2003). *Langmuir*, *19*, 160.
[22] Boehm, H. P., & Herrmann, M. (1967). *Z. Anorg. Allg. Chem.*, *352*, 156.
[23] Zubowa, H.-L., Kosslick, H., Carius, E., Frunza, S., Frunza, L., Landmesser, H., Richter, M., Schreier, E., & Fricke, R. (1998). *Micropor. Mesopor. Mater.*, *21*, 467.
[24] Hanawa, T., & Ota, M. (1992). *Appl. Surf. Sci.*, *55*, 269.
[25] Marino, C. E. B., Nascente, P. A. P., Biaggio, S. R., Rocha-Filho, R. C., & Bocch, N. (2004). *Thin Solid Films*, *468*, 109.
[26] Batzill, M., Morales, E. H., & Diebold, U. (2007). *Chem. Phys.*, *339*, 36.
[27] Luca, D., Macovei, D., & Teodorescu, C.-M. (2006). *Surf. Sci.*, *600*, 4342.
[28] McCafferty, E., & Wightman, J. P. (1998). *Surf. Interface Anal.*, *26*, 549.
[29] Pouilleau, J., Devilliers, D., Garrido, F., & Durandvidal, S. (1997). *Mater. Sci. Eng.*, *47*, 235.
[30] Sodhi, R. N. S., Weninger, A., Davis, J. E., & Sreenivas, K. (1991). *J. Vac. Sci. Technol. A*, *9*, 1329.
[31] Young-Taeg, S., Johansson, C. B., Petroni, S., Krozer, A., Jeong, Y., Wennerberg, A., & Albrektsson, T. (2002). *Biomaterials*, *23*, 491.
[32] Godfroid, T., Gouttebaron, R., Dauchot, J. P., Lecle′re Ph., & Lazzaroni, R. (2003). *Thin Solid Films*, *437*, 57.
[33] Simmons, G. W., & Beard, B. C. (1987). *J. Phys. Chem.*, *91*, 1143.
[34] Sanjines, R., Tang, H., Berger, F., Gozzo, F., Margaritondo, G., & Levy, F. (1994). *J. Appl. Phys.*, *75*, 2945.

[35] Riakar, G. N., Gregory, J. C., Ong, J. L., Lucas, L. C., Lemons, J. E., Kawahara, D., & Nakamura, M. (1995). *J. Vac. Sci. Technol. A*, *13*, 2633.
[36] Nesbitt, H. W., Bancroft, G. M., Henderson, G. S., Ho, R., Dalby, K. N., Huang, Y., & Yan, Z. (2011). *J. Non-Cryst. Solids*, *357*, 170.
[37] Perron, H., Vandenborre, J., Domain, C., Drot, R., Roques, J., Simoni, E., Ehrhardt, J.-J., & Catalette, H. (2007). *Surf. Sci.*, *601*, 518.
[38] Gao, X., Simon, R. B., Fierro, J. L. G., Banares, M. A., & Wachs, I. E. (1998). *J. Phys. Chem. B*, *102*, 5653.
[39] Scofield, J. H. (1976). *J. Electron Spectrosc.*, *8*, 129.
[40] Sham, T. K., & Lazarus, M. S. (1979). *Chem. Phys. Lett.*, *68*, 426.
[41] Wang, L.-Q., Baer, D. R., Engelhard, M. H., & Shultz, A. N. (1995). *Surf. Sci.*, *344*, 237.
[42] Ketteler, G., Yamamoto, S., Bluhm, H., Andersson, K., Starr, D. E., Ogletree, D. F., Ogasawara, H., Nilsson, A., & Salmeron, M. (2007). *J. Phys. Chem. C*, *111*, 8278.
[43] Lindberg, B., Svensson, S., Malmquist, P. A., Basilier, E., Gelius, U., & Siegbahn, K. (1976). *Chem. Phys. Lett.*, *40*, 175.
[44] Huang, M., Adnot, A., & Kaliaguine, S. (1993). *J. Chem. Soc. Faraday Trans.*, *89*, 4231.
[45] Borade, R., Adnot, A., & Kaliaguine, S. (1990). *J. Mol. Catal.*, *61*, 7.
[46] Bezrodna, T., Puchkovska, G., Shymanovska, V., Baran, J., & Ratajczak, H. (2004). *J. Molec. Struct.*, *700*, 175.
[47] Busani, T., & Devine, R. A. B. (2005). *Semicond. Sci. Technol.*, *20*, 870.
[48] Martra, G. (2000). *Appl. Catal. A: General*, *200*, 275.
[49] Primet, M., Pichat, P., & Mathieu, M.-V. (1971). *J. Phys. Chem.*, *75*, 1216.
[50] Morterra, C. (1988). *J. Chem. Soc., Faraday Trans.*, *84*, 1617.
[51] Henderson, M. A. (1996). *Langmuir*, *12*, 5093.
[52] Deiana, C., Fois, E., Coluccia, S., & Martra, G. (2010). *J. Phys. Chem. C*, *114*, 21531.
[53] Cerrato, G., Marchese, L., & Morterra, C. (1993). *Appl. Surf. Sci.*, *70/71*, 200.
[54] Tanaka, K., & White, J. M. (1982). *J. Phys. Chem.*, *86*, 4708.
[55] Maira, A. J., Coronado, J. M., Augugliaro, V., Yeung, K. L., Conesa, J. C., & Soria, J. (2001). *J. Catal.*, *202*, 413.
[56] Gnatyuk, I., Puchkovskaya, G., Yaroshchuk, O., Goltsov, Y., Matkovskaya, L., Baran, J., Morawska-Kowal, T., & Ratajczak, H. (1999). *J. Mol. Struct.*, *511/512*, 189.
[57] Gnatyuk, I., Puchkovska, G., Chashechnikova, I., Nozirov, F., Jurga, S., & Peplinska, B. (2004). *J. Mol. Struct.*, *700*, 183; Chashechnikova, I., Dolgov, L., Gavrilko, T., Puchkovska, G., Ye. Shaydyuk, Lebovka, N., Moraru, V., Baran, J., & Ratajczak, H. (2005). J. Mol. Struct., 744–747, 563.
[58] Frunza, L., Kosslick, H., Bentrup, U., Pitsch, I., Fricke, R., Frunza, S., & Schönhals, A. (2003). *J. Mol. Struct.*, *341*, 651.
[59] Frunza, L., Frunza, S., Poterasu, M., Beica, T., Kosslick, H., & Stoenescu, D. (2009). *Spectrochimica Acta Part A*, *72*, 248; Frunza, S., Schönhals, A., Frunza, L., Beica, T., Zgura, I., Ganea, P., & Stoenescu, D. (2010). *Chem. Phys., 372*, 51.
[60] (a) Puchkovskaya, G. A., Reznikov, Yu. A., Yakubov, A. A., Yaroshchuk, O. V., & Glushchenko, A. V. (1996). *J. Mol. Struct.*, *381*, 133; (b) Puchkovskaya, G. A., Reznikov, Yu. A., Yakubov, A. A., Yaroshchuk, O. V., & Glushchenko, A. V. (1997). *J. Mol. Struct.*, *404*, 121; (c) Babkov, L. M., Gnatyuk, I. I., & Trukhachev, S. V. (2005). *J. Mol. Struct.*, *744–747*, 425.
[61] Leyte, J. C., Jesse, W., Leyte-Zuiderweg, L. H., & van Woerkom, P. C. M. (1998). *J. Phys.: Condens. Matter*, *10*, 11617.
[62] Tanaka, H., Inagaki, S., Fukishima, Y., & Kaneko, K. (2000). *Stud. Surf. Sci. Catal.*, *129*, 623.
[63] (a) Leadbetter, A. J., Richardson, R. M., & Colling, C. N. (1975). *J. Phys. Colloque C1*, *36*, 37; (b) Lydon, J. E., & Coacley, C. J. (1975). *J. Phys.*, *36*, 45.
[64] Zecchina, A., Guglielminotti, E., Coluccia, S., Borello, E. (l969). *J. Chem. Soc. A*, *1969*, 2169–2199.
[65] Neto, A. R. R., & Leite Alves, H. W. (2010). *Phys. Status Solidi C*, *7*, 308.
[66] Lu, H. M., Wen, Z., & Jiang, Q. (2005). *Chem. Phys.*, *309*, 303.